Uncooled infrared detectors for 3–5 μm and beyond

P. V. V. Jayaweera,[1] S. G. Matsik,[1] A. G. U. Perera,[1,a)] H. C. Liu,[2] M. Buchanan,[2] and Z. R. Wasilewski[2]
[1]*Department of Physics and Astronomy, Georgia State University, Atlanta, Georgia 30303, USA*
[2]*Institute for Microstructural Sciences, National Research Council, Ottawa Ontario K1A 0R6, Canada*

(Received 20 May 2008; accepted 24 June 2008; published online 15 July 2008)

Avoiding cryogenic cooling not only reduces the cost and weight but also simplifies the infrared detector system allowing widespread usage. Here an uncooled infrared detection using intravalence bands is reported. A set of three *p*-GaAs/$Al_xGa_{1-x}As$ multiple heterojunction detector structures were used to demonstrate the concept experimentally. A preliminary detector showed peak responsivity of 0.29 mA/W at 2.5 μm at 300 K. The intravalence band approach can be used to cover various wavelength ranges by using different material systems giving rise to the possibilities of a dual band detector operating in atmospheric windows. © *2008 American Institute of Physics*. [DOI: 10.1063/1.2959060]

Initial photoconductive IR detectors have been developed utilizing band-to-band transitions or dopant-to-band transitions. The band-to-band detectors typically require semiconductors whose band edge is close to the energy of the photon to be detected. For the IR region of the spectrum, such detectors are typically fabricated in materials which have difficulties associated with the quality. HgCdTe and InSb are interesting materials that have been studied[1] for a long time for both photoconductive and photovoltaic modes. Cryogenically cooled HgCdTe has a broad response range from 1 to 20 μm, and InSb responds up to 5.5 μm. Research is in progress to achieve uncooled HgCdTe detectors.[2] Extended InGaAs *p-i-n* photodiodes responding up to 2.6 μm are commercially available. On the other hand, dopant-to-band detectors operate at very low temperature. In order to overcome the limitations of those two methods intersubband transition based detectors were introduced about two decades ago. The quantum well detectors utilize intersubband transitions with the restriction of absorbing normal incident radiation due to the selection rules.[3] Hence these detectors require 45° coupling or a corrugated surface (for grating coupling). Furthermore, quantum efficiency is further reduced due to the selection rule utilizing only one polarization of light. Later, homojunction[4] and heterojunction[5] interfacial workfunction internal photoemission detectors were introduced. Those utilized intraband transitions [light hole (L-H) to heavy hole (H-H) transition] and are free of selection rule limitations. As the free carrier absorption is proportional to the square of the wavelength,[6] the detector response is better at longer wavelengths. Highly *p*-doped GaAs exhibits enhanced absorption around 2–4 μm range beyond the free carrier absorption due to L-H/H-H to split-off (S-O) transitions. The S-O band effects have been experimentally observed in the emission of GaAs metal semiconductor field effect transistors[7] and have enhanced the response of GaInAsP[8] quantum wells and GaAs[9] quantum wells. Extensive theoretical studies on the importance of the spin S-O band and the tunneling properties of the holes through $Al_xGa_{1-x}As$/GaAs heterostructures is reported elsewhere.[10] Here a GaAs based S-O band detector responding in 2–4 μm at ambient temperature is reported.

The active region of the detector consists of multiple periods of *p*-doped GaAs emitter and $Al_xGa_{1-x}As$ barrier regions sandwiched between two highly doped contact layers. The emitter layers are doped high enough to have the scattering length similar to the emitter thickness, so that carriers will scatter before the wave function interferes with itself. Hence this structure will not form discrete quantum states inside the wells. This makes the carrier distribution in the emitter three dimensional but still bound. A band diagram (*E-k*) for an emitter region of the detector is shown in Fig. 1. In order to explain the detection mechanism, three valence bands will have to be considered, as shown in Fig. 1, the L-H and H-H bands which are degenerate at $k=0$, and the S-O band which is separated from them by an energy $E_{E\text{-SO}}$. Under equilibrium conditions, a *p*-doped region will have a Fermi level in the L-H and H-H bands, but above the S-O band maximum. The detector mechanism can be divided into three main processes: (I) photoabsorption, which produces the excited carriers, (II) escape of the carriers, and (III) the sweep out and collection of the escaped carriers. The arrows in the Fig. 1 indicate the possible threshold transition mechanisms. These transitions could be direct or indirect. Once the carrier is in the S-O band, it can escape directly or scatter

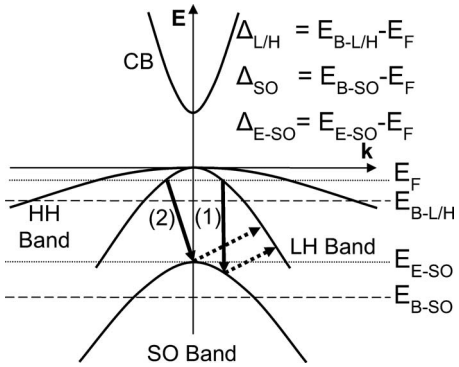

FIG. 1. A band diagram for an emitter region of the detector, illustrating the different IR detection threshold mechanisms. The horizontal dashed lines $E_{B\text{-}L/H}$ and $E_{B\text{-}SO}$ indicate the L-H/H-H and S-O band maximum ($k=0$) positions in the barrier. The horizontal dotted lines E_F and $E_{E\text{-}SO}$ indicate the Fermi energy and the S-O energy at $k=0$.

a)Electronic mail: uperera@gsu.edu.

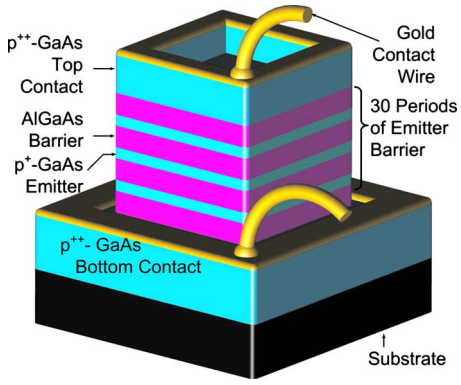

FIG. 2. (Color online) A mesa of the processed detector showing the window etched into the top contact for front-side illumination. There were 30 periods consisting of 3×10^{18} cm^{-3} p-doped 188 Å GaAs emitters and 600 Å $Al_{0.57}Ga_{0.43}As$ barriers. Part of the bonded contact wires also shown here.

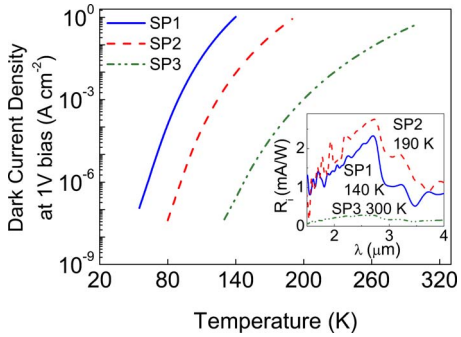

FIG. 3. (Color online) The dark current density vs temperature for samples SP1, SP2, and SP3 under 1 V applied bias. The samples SP1, SP2, and SP3 have barriers with aluminum fractions 0.28, 0.37, and 0.57 respectively. Inset shows the responsivities of the SP1, SP2, and SP3 at 140, 190, and 300 K respectively, i.e., close to optimum operating temp for each sample, reaching a 1 A/cm^2 dark current density value.

back into the L-H/H-H bands and then escape. For a direct transition (shown by arrow 1 solid part) there is no phonon involved so k is conserved. The excited carrier then must scatter back to the L-H band (or possibly the H-H band although this involves much higher k changes) in order to escape. This phonon involved scattering is shown by the dashed arrow. The threshold for this process is determined by the difference of energy in the light and S-O hole bands at k corresponding to the Fermi energy shown by E_F in the Fig. 1. For the indirect transition (shown by arrow 2) a phonon is involved and higher energies are possible. The high energy transition which is below the barrier in the S-O band could escape directly. (It is not shown as this is a purely spatial change and does not affect the k-space picture.) The indirect absorption has two thresholds. For escape with a scattering it is the difference of the Fermi energy and the S-O band at $k=0$ in the emitter ($\Delta_{E\text{-SO}}$). For escape without scattering, it is the difference between the Fermi energy and the S-O band at $k=0$ in the barrier (Δ_{SO}). The horizontal dashed lines $E_{B\text{-L/H}}$ and $E_{B\text{-SO}}$ indicate the L-H/H-H and S-O band maximum (at $k=0$) level in the $Al_xGa_{1-x}As$ barrier. The horizontal dotted lines E_F and $E_{E\text{-SO}}$ indicate the Fermi energy and the S-O energy at $k=0$. Even though Δ_{SO} is constant for a given material system, $\Delta_{L/H}$ (also known as free carrier threshold) can be adjusted by varying Al fraction x and the doping concentration of the emitter layer.[5] The $\Delta_{\text{L/H}}$ is the lowest barrier for the excited carriers in L-H/H-H bands, which determine threshold wavelength for the free carrier mechanism and also major contribution for dark current hence determined maximum operating temperature. By making $\Delta_{\text{L/H}}$ larger it is possible to make S-O transitions as dominant detection mechanism and increase operating temperature. However, higher $\Delta_{\text{L/H}}$ can lead to lower the response by reducing escape probability of impact ionized carriers due to high-energy photons.

The detector structures SP1, SP2, and SP3 with three different $\Delta_{\text{L/H}}$ values of 155, 207, and 310 meV (corresponding Al fractions for those $\Delta_{\text{L/H}}$ values are $x=0.28, 0.37, 0.57$ giving threshold wavelengths of 8, 6, and 4 μm) were grown on semi-insulating GaAs substrates with a 0.7 μm thick bottom contact layer, of 1×10^{19} cm^{-3} p-doped GaAs followed by 30 periods of a 600 Å undoped $Al_xGa_{1-x}As$ barrier and 3×10^{18} cm^{-3} p-doped 188 Å GaAs emitter. The last emitter was 0.2 μm thick and p-doped to 1×10^{19} cm^{-3} in order to use as top contact layer. The detectors were processed by wet etching to form square mesas with sides 400, 600, 800, and 1000 μm. Ti/Pt/Au ohmic contacts were evaporated onto the top and bottom contact layers. A ring contact was used on the top surface and a window was opened through the top contact for front-side illumination. The sample pieces with $\sim4\times8$ mm^2 dimensions and 10–12 different sized mesas were mounted on standard chip carriers and gold wires were wire bonded from top and bottom electrical connections. A schematic of a single mesa of the detector is shown in Fig. 2. The current voltage (I-V) characteristics were measured with different temperatures from 70 to 300 K. As shown in Fig. 3, dark current density at 1 V bias reached the same order at 140, 190, and 300 K for samples SP1, SP2, and SP3, respectively. Comparison of the measured dynamic resistance and dark current density for the three samples are presented in Table I. The spectral response of the detectors SP1, SP2, and SP3 were measured using a Fourier transform IR spectrometer (PerkinElmer system2000) at temperatures up to 140, 190, and 300 K, respectively. Inset in Fig. 3 shows responsivity calibrated using a bolometer for each detector under 4 V bias. These responsivities were also verified with calibrated InGaAs photo diode at 2.5 μm. Figure 4 shows the responsivity of the detector SP3 at 300 K under four different biases with the maximum responsivity of 0.29 mA/W at 300 K and 2.5 μm. The noise current density was measured using a dynamic signal analyzer (Stanford Research SR785) with the sample mounted in an optically and electrically shielded dewar. Batteries were used to bias the sample to minimize noise components from the bias source. Majority of noise is believed to be generation recombination and Johnson noise. Normalized detectivity (D^*) was obtained using the formula $D^*=(R\times\sqrt{A})/I_N$. Where R is the responsiv-

TABLE I. Sample parameters at maximum operating temperatures (T_{max}). The dynamic resistance (R_{Dyn}), dark current density (I_{Dark}) at 1 V bias and D^* are experimentally measured values. $\Delta_{\text{L/H}}$ is the designed band offset.

Sample	$\Delta_{\text{L/H}}$ (eV)	T_{max} (K)	R_{Dyn} (Ω)	I_{Dark} (A cm^{-2})	D^* (Jones)
SP1	0.155	140	787	0.663	2.1×10^6
SP2	0.207	190	913	0.875	1.8×10^6
SP3	0.310	300	1138	0.563	6.8×10^5

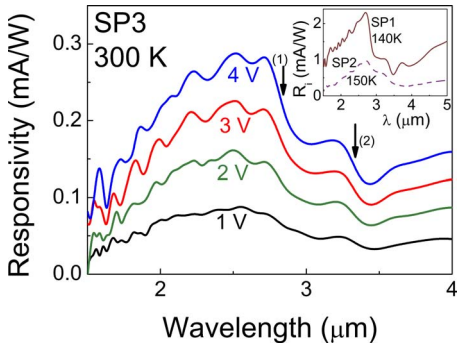

FIG. 4. (Color online) The measured responsivity of the sample SP3 under four different biases at 300 K showing peaks around 2.5 μm. The arrows 1 and 2 indicate the thresholds at 2.9 and 3.4 μm corresponding to the transitions 1 and 2, as shown in Fig. 1. The inset shows the responsivity of the samples SP1 and SP2 at 140 and 150 K, respectively.

ity (in A W^{-1}), A is the optically active area of the detector (in cm^2) and I_N is the noise current density (in A $Hz^{-1/2}$). The calculated D^* values for each sample at the maximum operating temperature is listed in Table I. The response observed in the sample SP3 at room temperature appears to be due to a single emitter with the other emitters not contributing. Modifications in the design to activate more emitters would lead to increase gain hence improved response. As shown in Fig. 4 the responsivity increases with the bias up to 4 V, but increased dark current (low dynamic resistance) reduced the response above 4 V bias. Even though the reported curves are at 300 K, response have also been observed up to 330 K by heating the sample stage using built-in heater. At 330 K dynamic resistance was reduced to several hundreds of ohms and the measured signal deteriorates almost to the noise level. The threshold wavelengths for the response mechanisms 1 and 2 shown in Fig. 2 can be identified in Fig. 4 at 2.9 and 3.4 μm, respectively. At 300 K mechanism (1) becomes dominant, as can be seen by the much larger step at 2.9 μm. The threshold for the free carrier response increased slowly with temperature due to increased number of carriers above the Fermi energy, which can give response at longer wavelengths. SP1 and SP2 detectors gave maximum operating temperatures 140 and 190 K, respectively. The higher responsivity and D^* was seen for longer wavelength threshold samples, possibly due to impact ionization (gain), compared to the shorter threshold samples, as shown in the inset of the Fig. 4. In order to increase the uncooled response of the S-O detectors, the gain must be increased. The limiting factor on gain in the present design is the trapping due to scattering between hot and cold carriers as the holes pass through the emitter layers. For a detector with a free carrier threshold near 4 μm, nearly 100% of the carriers will be trapped and then reemitted at the barrier. This effectively limits the gain for the detector as a whole to $1/N$, where N is the number of emitter periods. One possible approach would be to use graded barriers with the higher Al fraction on the end toward the collector contact. The difference in barrier heights on opposite sides of the emitters would reduce the trapping from the scattering and should lead to an increased gain. Initial estimates indicate that such an approach could lead to an increase in the gain of a factor 50 at the optimum bias.

An uncooled IR detector based on GaAs/AlGaAs multiple heterostructure responding up to 4 μm was reported. The response is primarily from H-H/L-H to S-O transitions and the detector shows peak D^* of 6.8×10^5 Jones, 2.5 μm, 300 K. As a well developed material system, GaAs is a feasible solution to the future of uncooled IR detection; hence high quality growing and integration with other readout electronics readily available. Materials other than GaAs/AlGaAs may lead to extend the coverage at longer wavelengths. Possible materials such as InP with a threshold of 11 μm and the nitride materials may be able to operate at 60 μm or beyond at elevated temperatures. Another possibility is to design a dual band detector that covers 3–5 and 8–14 μm atmospheric windows using a combined system with arsenides and phosphides.

This work was supported in parts by the US NSF under Grant No. ECS-0553051.

[1]A. Rogalski, Prog. Quantum Electron. **27**, 59 (2003).
[2]A. Piotrowski, P. Madejczyk, W. Gawron, K. Klos, J. Pawluczyk, J. Rutkowski, J. Piotrowski, and A. Rogalski, Infrared Phys. Technol. **49**, 173 (2007).
[3]D. D. Coon and R. P. G. Karunasiri, Appl. Phys. Lett. **45**, 649 (1984).
[4]A. G. U. Perera, H. X. Yuan, and M. H. Francombe, J. Appl. Phys. **77**, 915 (1995).
[5]A. G. U. Perera, S. G. Matsik, B. Yaldiz, H. C. Liu, A. Shen, M. Gao, Z. R. Wasilewski, and M. Buchanan, Appl. Phys. Lett. **78**, 2241 (2001).
[6]A. L. Korotkov, A. G. U. Perera, W. Z. Shen, J. Herfort, K. H. Ploog, W. J. Schaff, and H. C. Liu, J. Appl. Phys. **89**, 3295 (2001).
[7]K. S. Zhuravlev, V. A. Kolosanov, A. G. Milekhin, V. G. Polovinkin, T. S. Shamirzaev, Yu N. Rakov, Yu B. Myakishev, J. Fryar, E. McGlynn, and M. O. Henry, Semicond. Sci. Technol. **19**, S94 (2004).
[8]J. R. Hoff, M. Razeghi, and G. J. Brown, Phys. Rev. B **54**, 10773 (1996).
[9]B. W. Kim, E. Mao, and A. Majerfeld, J. Appl. Phys. **81**, 1883 (1997).
[10]S. Ekbote, M. Cahay, and K. Roenker, Phys. Rev. B **58**, 16315 (1998).